Available online at www.sciencedirect.com

SciVerse ScienceDirect

Ceramics International 39 (2013) 219–225

CERAMICS INTERNATIONAL

www.elsevier.com/locate/ceramint

Fatigue improvement in modified lead zirconate titanate ceramics through employment of $La_{0.8}Sr_{0.2}MnO_3$ buffer layers

Baohua Wen[a], Yong Zhang[b,*], Xiaolin Liu[a], Liang Ma[b], Xiangrong Wang[b]

[a]*State Key Laboratory of Organic–Inorganic Composites, Beijing University of Chemical Technology, Beijing 100029, China*

[b]*Beijing Fine Ceramics Laboratory, State Key Laboratory of New Ceramics and Fine Processing, Institute of Nuclear and New Energy Technology, Tsinghua University, Beijing 100084, China*

Received 20 March 2012; received in revised form 26 May 2012; accepted 4 June 2012
Available online 13 June 2012

Abstract

The dielectric, ferroelectric and fatigue properties of modified lead zirconate titanate (PZT) ceramics were investigated in terms of the effect of $La_{0.8}Sr_{0.2}MnO_3$ (LSM) buffer layers. The double sided LSM buffer layers resulted in a lower dielectric loss, a weaker frequency dependence of dielectric constant, a lower leakage current density, and an increase in the saturation polarization. Moreover, it was found that up to 1.4×10^7 cycle numbers, the Ag||LSM/PZT/LSM||Ag capacitor, with remanent polarization decreased by 55%, was superior to the Ag||PZT||Ag capacitor by 85%. The results indicate that the LSM buffer layers can improve the fatigue endurance of the PZT ceramics with Ag electrodes, mainly because the accumulated charges were compensated at the interface junctions between the LSM buffer layers and the Ag electrodes. We fit the polarization fatigue data using a modified model and calculated the characteristic decay time of oxygen vacancy migration in the Ag||LSM/PZT/LSM||Ag and the Ag||PZT||Ag capacitors, respectively.

Keywords: C. Fatigue; Ferroelectric; Buffer layer; Ceramics

1. Introduction

Several groups of ferroelectric materials have attracted great attention in the past several decades for many technologically valuable applications, such as nonvolatile ferroelectric random access memories, sensors, and micro-electromechanical systems (MEMS) [1–3]. Among many families of ferroelectrics, $Pb(Zr,Ti)O_3$ (PZT) is one of the most widely studied materials for these applications, considering its large remanent polarization, excellent dielectric, ferroelectric and piezoelectric properties.

Nevertheless, PZT materials with metal electrodes suffer a significant polarization fatigue against repeated polarization switching, so there have been many studies concerning this problem. A number of microscopic origins for the fatigue phenomena have been proposed. In general, the purely mechanical source of microcracking has been assumed to be the major origin of fatigue in bulk ceramics [4,5]. Grossmann et al. [6] have proposed a model for imprint in PZT thin films. They suggest in the model that imprint is caused by a strong electric field within a thin surface layer in which the ferroelectric polarization is smaller or even absent compared to the bulk of the film. These interface scenarios can be either a space charge layer or a chemically or mechanically distorted layer, which does not take part in the polarization reversal process. A point defect model is proposed to calculate the migration of electronic and ionic defects under the dc field as well as the current response of the system [7]. Moreover, many studies have tended to explain the fatigue as a consequence of domain wall pinning [8] and domain nucleation suppression [9] at electrode–ceramics interfaces especially in thin films. There have been many earlier attempts to decrease the rate of fatigue degradation. The method of using conducting oxide electrodes such as $La_{0.5}Sr_{0.5}CoO_3$ [10], $LaNiO_3$ [11], $SrRuO_3$ [12], $La_{0.7}Sr_{0.3}MnO_3$ [13], or RuO_2 [14] was implemented. It is reported that these oxides reduce long-range migration of oxygen vacancies during cycling, thereby improving the fatigue endurance of ferroelectric capacitors.

*Corresponding author. Fax: +86 10 89796022.
E-mail address: yzhang@tsinghua.edu.cn (Y. Zhang).

0272-8842/$36.00
http://dx.doi.org/10.1016/j.ceramint.2012.06.012

In recent years, some oxide buffer layers such as $(Ba_{0.5}Sr_{0.5})TiO_3$ [15], $(Pb_{0.72}La_{0.28})Ti_{0.93}O_3$ [16], $BaPbO_3$ [17], $PbZrO_3$ [18], $(Bi_{3.15}Nd_{0.85})Ti_3O_{12}$ [19] and $Bi_{3.25}La_{0.75}Ti_3O_{12}$ [20] have attracted considerable interest for practical applications in PZT thin films, because they provide better fatigue endurance characteristics and have similar structure with the ferroelectric thin films. However, there are a few attempts focused on improving fatigue endurance properties of ferroelectric ceramics by employing $La_{0.8}Sr_{0.2}MnO_3$ buffer layers.

In this work, the dielectric properties, leakage current, polarization–electric field (*P–E*) loops and fatigue characteristics of the modified PZT ceramics with and without $La_{0.8}Sr_{0.2}MnO_3$ (LSM) buffer layers have been investigated with the comparative analysis of experimental data. The LSM buffer layers were deposited on both sides of the modified PZT ceramics via a screen printing method. The choice of the LSM material is due to its high conductivity and similar crystal structure with the modified PZT ceramics.

2. Experimental procedures

The modified PZT ceramic samples and LSM powders with the compositions of $Pb_{0.96}Sr_{0.04}$ $(Mg_{1/3}Nb_{2/3})_{0.275}(Ni_{1/3}Nb_{2/3})_{0.1}Ti_{0.375}Zr_{0.25}O_3$ and $La_{0.8}Sr_{0.2}MnO_3$ were made by standard solid state reactions. For the modified PZT ceramics, the raw materials used were reagent grade Pb_3O_4, ZrO_2, TiO_2, $SrCO_3$, $MgCO_3 \cdot Mg(OH)_2 \cdot 5H_2O$, $Ni(Ac)_2$ and Nb_2O_5. The purity of the starting raw materials was 99.0%. In addition, 1.5 wt% extra Pb_3O_4 was added to compensate for PbO volatility. These weighted powders were mixed with yttria-stabilized zirconia balls and alcohol as the milling media for 6 h. After drying, these homogeneous mixtures were sieved and then calcined at 800 °C for 2 h. The calcined powders were subsequently ball-milled in the same media for 6 h, dried and sieved once more. To obtain ceramics, the milled powders were mixed with a 3 wt% polyvinyl alcohol binder and then pressed into pellets with a diameter of 15 mm and a thickness of 1.2 mm at a uniaxial pressure of 4 MPa. Following binder burnout at 450 °C, the pressed pellets were then sintered in air at 1070 °C for 2 h using sealed alumina crucibles.

For the LSM powders, Lanthanum nitrate $(La(NO_3)_3 \cdot 6H_2O$, AR), strontium nitrate $(Sr(NO_3)_2$, AR) and manganous nitrate $(Mn(NO_3)_2$, 50% aqueous solution) were used as raw materials. The powder mixture was calcined at 900 °C for 2 h. The calcined powders mixed with an organic binder were used as the inks for screen-printing deposition. To obtain LSM/PZT/LSM ceramics, LSM buffer layers were directly deposited on both sides of the PZT ceramics via the screen printing method. The modified PZT ceramics with the LSM buffer layers were then sintered at 950 °C for 2 h in air. The thickness of LSM is about 5 μm. Before the screen-printing deposition experiment, the samples were polished to form pellets with a thickness of 1 mm, then painted with silver pastes on both sides of the PZT and LSM/PZT/LSM ceramics followed by firing at 600 °C for 20 min. Thus, the target Ag||PZT||Ag and Ag||LSM/PZT/LSM||Ag capacitors were obtained, respectively.

The microstructure observation and analysis of the fracture surfaces of the ceramic specimens were performed with a scanning electron microscope (SEM: FEI Qunanta 200 FEG). The dielectric properties were measured by a LCR meter (Model HP4284A Hewlett-Packard, Palo Alto, CA) at room temperature with the amplitude of 1 V from 25 Hz to 1 MHz. The *P–E* loops were measured using a Sawyer–Tower capacitive voltage divider in a computerized measuring system. All electric fields were supplied by a high voltage power supply (Trek 609-B, NY, USA) driven by a frequency generator (HP33220A, CA, USA). The electric field was applied from 1 kV/mm to 2 kV/mm at 1 Hz during measurements.

The leakage current test is carried out by a home-made measuring system. Before measuring the leakage current characteristics, the ferroelectric polarization was saturated by applying an electric field of 1.5 kV/mm and with the same polarity as that used for current measurements. In this way, the contribution of the current due to polarization reversal is minimized.

Fatigue was induced by employing the samples to bipolar voltage cycling under the sinusoidal electric field amplitude of 1.5 kV/mm and a frequency of 50 Hz. The samples were fixed on two spherical metal clamps and immersed in silicone oil to avoid arcing. And the samples can oscillate freely during fatigue experiment.

3. Results and discussion

The dielectric properties as a function of frequency for the Ag||LSM/PZT/LSM||Ag and the Ag||PZT||Ag capacitors were shown in Fig. 1. The dielectric constant-

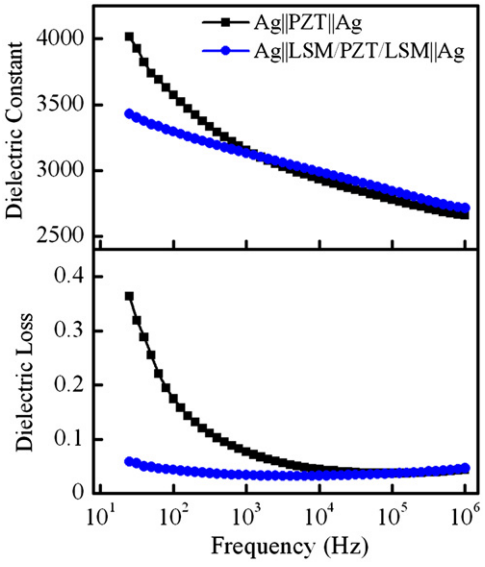

Fig. 1. Frequency dependence of the dielectric constant and dielectric loss for the Ag||LSM/PZT/LSM||Ag and the Ag||PZT||Ag capacitors.

frequency and the dielectric loss-frequency curves were measured at room temperature. Obviously, the dielectric constants of both capacitors decrease gradually with the increase of the frequency. Such an observation for the Ag||PZT||Ag capacitors, where a higher dielectric constant at a lower frequency region is accompanied by higher dielectric loss, is expected due to the increasing interfacial polarization contribution [21]. This result could be explained on the basis of the defect-related transport. By comparison, the dielectric constant and dielectric loss of the Ag||LSM/PZT/LSM||Ag capacitors showed relatively weak frequency dependence than that of the Ag||PZT||Ag capacitors as shown in Fig. 1. In the low frequency regime, the less frequency dispersive states in the Ag||LSM/PZT/LSM||Ag capacitors indicate better interfacial characteristics and lower defect concentrations, which are resulted from the introduction of LSM buffer layers between the PZT ceramics and the Ag electrodes. Similar phenomenon has been reported in the $Ba_{0.5}Sr_{0.5}TiO_3/Bi_{1.05}La_{0.05}FeO_3/Ba_{0.5}Sr_{0.5}TiO_3$ sandwich structures [22].

The leakage current density versus electric field (J–E) curves of the modified PZT ceramics without and with LSM buffer layers are presented in Fig. 2(a), which were measured in the range of 0.2–2 kV/mm. It can be seen that the Ag||LSM/PZT/LSM||Ag capacitor exhibits a lower leakage current density as compared with the Ag||PZT||Ag capacitor, in agreement with their P–E hysteresis loops and dielectric measurements shown above. These results confirm that the leakage current of the modified PZT ceramics was suppressed by the inserted LSM buffer layers. In order to determine the leakage mechanism, ln(J) versus ln(E) curves of the modified PZT ceramics without and with LSM buffer layers were shown in Fig. 2(b). The ln(J) − ln(E) plots of leakage current density versus applied electric field indicate a characteristic of space charge limited conduction (SCLC) mechanism, which can be expressed as follows [23]:

$$J = \frac{9\mu\varepsilon_r\varepsilon_0\theta E^2}{8d} \quad (1)$$

where μ is the charge carrier mobility, ε_0 is the permittivity of free space, ε_r is the permittivity of the ceramic, θ is the ratio of the total density of the induced free carriers to the trapped carriers, and d is the ceramic thickness. Here the exponent is 2, but the defects in the crystal may affect the value of the exponent. The leakage current of the modified PZT ceramics without and with LSM buffer layers appears to increase almost linearly with a slope close to the unity. An experimental exponential value of 1.35 was obtained from the ln(J)–ln(E) plots shown in Fig. 2(b). The deviation may be due to the large amount of structural disorders present in the polycrystalline ceramics.

Fig. 3 shows the ferroelectric hysteresis (P–E) loops and switching current densities of the Ag||LSM/PZT/LSM||Ag and the Ag||PZT||Ag capacitors under a maximum field of 2 kV/mm. When the applied electric field is about 0.75 kV/mm (close to coercive field), the switching current densities exhibit a rapid increase, corresponding to the occurrence of polarization switching in the PZT ceramics, as shown in Fig. 3(blue line). It is known that the applied electric field can result in a change in the surface charges of the sample. One contribution is from the ferroelectric domain switching which can be represented by the sharp increase in the switching current density J, which

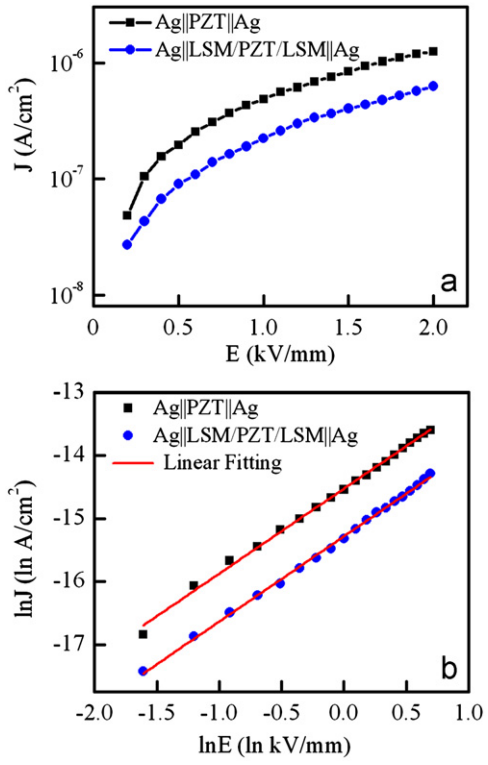

Fig. 2. (a) Leakage current density as a function of applied electrical field for the Ag||LSM/PZT/LSM||Ag and the Ag||PZT||Ag capacitors at room temperature and (b) ln(J)–ln(E) plots of leakage current density versus applied electric field.

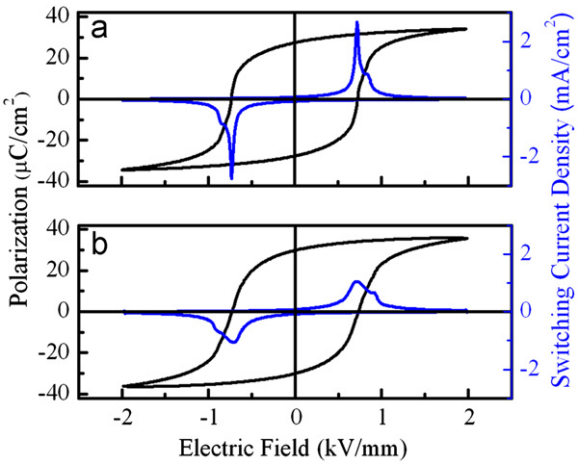

Fig. 3. P–E hysteresis loops and switching current densities of (a) the Ag||PZT||Ag and (b) the Ag||LSM/PZT/LSM||Ag capacitors versus electric field as measured at room temperature with a triangular wave at a measuring frequency of 1 Hz. (For interpretation of the references to color in this figure, the reader is referred to the web version of this article.)

can be calculated from the following equation:

$$J = A^{-1}\frac{dP}{dt} \tag{2}$$

As the polarization dynamics cease after a certain time, J subsides [23].

Ferroelectric loops were measured at room temperature with a frequency of 1 Hz. The remanent polarization and saturated polarization are 29.9 and 36.7 μC/cm^2 for the Ag||LSM/PZT/LSM||Ag capacitor and 27.5 and 34.1 μC/cm^2 for the Ag||PZT||Ag capacitor, respectively. It was found that compared with the Ag||PZT||Ag capacitor, the ferroelectric properties of the Ag||LSM/PZT/LSM||Ag capacitor can be improved, which were shown in Fig. 4. There are two kinds of reasons for high polarization in the Ag||LSM/PZT/LSM||Ag capacitor: one may be attributed to a relatively low concentration of defects, which may be related to the diffusion into the PZT bulk due to the high temperature (950 °C) processing of the LSM ceramics. The other is that LSM layers act as buffering layers to block the oxygen vacancy migration between the modified PZT ceramics and the Ag electrodes during electrical measurements.

Fig. 5 illustrates the evolution of polarization for the Ag||PZT||Ag and Ag||LSM/PZT/LSM||Ag capacitors as a function of switching cycle number during fatigue tests. It can be seen that a systematic decrease in the polarization and the hysteresis loop becomes squashed while the coercive field increases monotonically with increasing switching cycle. Moreover, the polarization amplitude decreased faster for the Ag||PZT||Ag capacitors, which will be discussed in the later part.

The scanning electron microscope (SEM) micrographs of the fracture surface for the fatigued (10^6 cycles) PZT samples without and with LSM buffer layers obtained in the experiments are shown in Fig. 6. It is confirmed in the present studies that the fatigued sample (after 10^6 cycles) revealed no microcracks underneath the electrodes. As shown in Fig. 6(b), a sandwich structure is observed in the fatigued sample with LSM buffer layers.

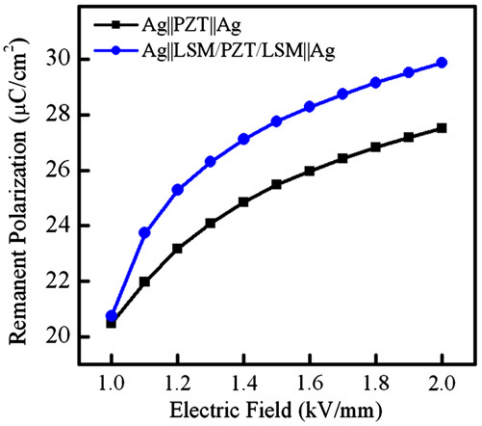

Fig. 4. The remanent polarization (Pr) values of the Ag||PZT||Ag and the Ag||LSM/PZT/LSM||Ag capacitors as a function of the maximum driving electric field.

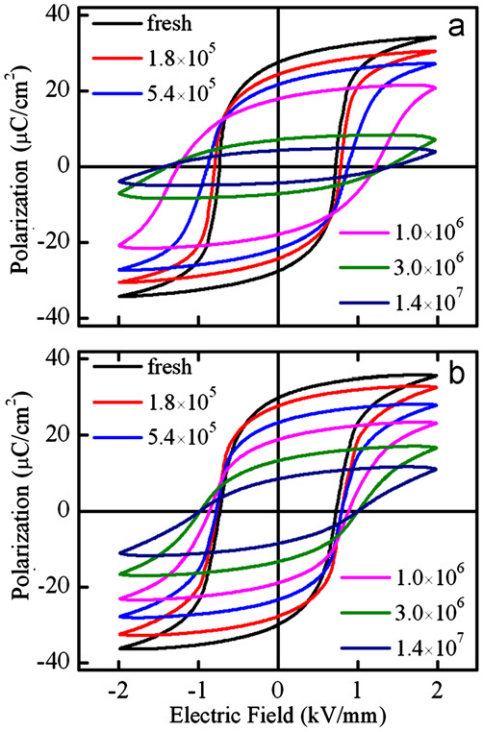

Fig. 5. P–E hysteresis loops of (a) the Ag||PZT||Ag and (b) the Ag||LSM/PZT/LSM||Ag capacitor samples after different cycles of polarization switching.

In order to study the effect of the buffer layer on the modified PZT ceramics, the fatigue behavior of the ceramic samples with and without buffer layers were investigated. Fig. 7 illustrates the normalized remanent polarization as a function of switching cycles for the Ag||LSM/PZT/LSM||Ag and the Ag||PZT||Ag capacitors. All the samples were cycled to 1.4×10^7 cycles under the bipolar electric field of 1.5 kV/mm. As shown in Fig. 7, the remnant polarization of the Ag||PZT||Ag capacitor rapidly degraded as expected (decreased by 85%). However, the modified PZT ceramics with the double-sided LSM buffer layers demonstrated better resistance to fatigue, which is only about 55% of the overall remnant polarization value lost after 1.4×10^7 switching cycles.

The polarization fatigue behavior can be majorly related to the kinetics of long-range diffusion of oxygen vacancies during the switching cycles. According to the Dawber and Scott fatigue model [24], mobile charged defects such as oxygen vacancies are easily migrated and accumulated at the regions near the electrodes during the switching process. This goes on to show that the net displacement of the mobile ions is the primary rate-limiting step in the fatigue process. The solid line shown in Fig. 7 is an empirical fit to experiment data so that,

$$P(N) = A\exp\left[-\tau^{-1}\frac{N}{f}\right] + B \tag{3}$$

where the constant A represents the fractions of polarization which can be pinned easily, while the constant B

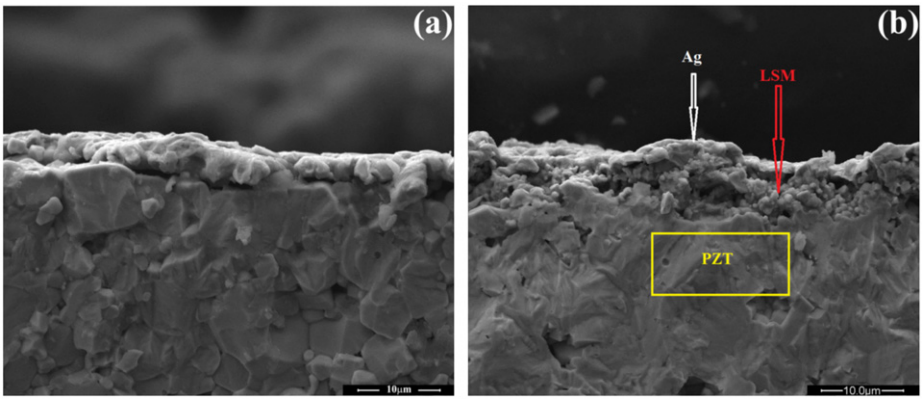

Fig. 6. SEM micrographs of the fracture surface for the fatigued (10^6 cycles) PZT samples (a) without and (b) with LSM buffer layers.

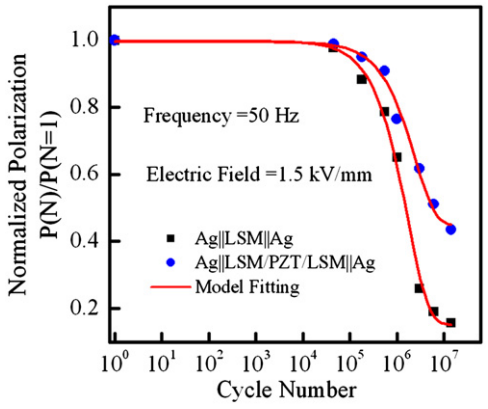

Fig. 7. Polarization fatigue measurements for the Ag||LSM/PZT/LSM||Ag and the Ag||PZT||Ag capacitors performed at room temperature. (For interpretation of the references to color in this figure legend, the reader is referred to the web version of this article.)

represents the fractions of polarization which cannot be pinned by the oxygen vacancy or injected electric charge ($A+B\sim1.0$). N is the cycle number, f is the frequency (Hz), and τ is the characteristic decay time.

With the above parameters, Eq. (3) can be applied to fit the measured fatigue data with only three parameters, A, B, and τ. Table 1 lists the fitted parameters for the Ag||LSM/PZT/LSM||Ag and the Ag||PZT||Ag capacitors. The fitted results are presented in Fig. 7(red lines) for the Ag||LSM/PZT/LSM||Ag and the Ag||PZT||Ag capacitors, respectively. It is shown that the modified model describes quite well the measured fatigue data for the two kinds of ceramics at room temperature. The long-range migration of oxygen vacancies in ceramics and, consequently, the domain pinning by these vacancies as the dominant origin of polarization fatigue in perovskite type ferroelectric ceramics, is demonstrated.

Looking at the fitting parameters in detail, it can be seen that characteristic decay time $\tau=4.8\times10^4$ s for the Ag||LSM/PZT/LSM||Ag capacitors is higher than $\tau=3.4\times10^4$ s for the Ag||PZT||Ag capacitors, indicating a

Table 1
Fitting parameters of Eq. (3) from the polarization fatigue data.

Materials	A	B	τ (s)	R^2
Ag||LSM/PZT/LSM||Ag	0.55	0.45	4.8×10^4	0.987
Ag||PZT||Ag	0.85	0.15	3.4×10^4	0.994

lower mobility for oxygen vacancies in the Ag||LSM/PZT/LSM||Ag capacitors than in the Ag||PZT||Ag capacitors at room temperature. This presents an intrinsic reason for the fact: the Ag||LSM/PZT/LSM||Ag capacitors show better fatigue-resistance than the Ag||PZT||Ag capacitors in spite of a much higher density of vacancies in the Ag||LSM/PZT/LSM||Ag capacitors. Therefore, it becomes obvious that parameter A is larger for the Ag||PZT||Ag capacitors and parameter B is larger for the Ag||LSM/PZT/LSM||Ag capacitors, noting that parameter A stands for the fraction of polarization destroyed after an extremely large N [25]. In details, for the Ag||PZT||Ag capacitors, $A\sim0.85\gg B\sim0.15$, reveals that in the initial state, most of the domains can be switched and are gradually pinned by the aggregated vacancies through the long-range diffusion. These domains would be finally pinned by the highly aggregated vacancies and become no more switched due to the polarization fatigue effect. On the contrary, for the Ag||LSM/PZT/LSM||Ag capacitors, $A\sim0.55>B\sim0.45$, means that in the initial state quite a number of domains are already slightly pinned by the high-density oxygen vacancies. Our results indicate that drift of charged species plays an important role in determining the polarization decay curve and constitute a test for fatigue models involving drift and diffusion of charged species.

On the other hand, these results can be explained by the La component of the LSM buffer layers which act as dopant [26]. La exists in the form of La^{3+}, which may diffuse into the PZT bulk due to the high temperature (950 °C) processing of buffer layers. And this donor doping can help to reduce or compensate for the Pb-site vacancies as well as the oxygen vacancies which can be created with PbO volatilization at high temperature

sintering process, therefore, the LSM buffer layers are considered to be diffusion barriers for the migration of oxygen vacancies in the LSM/PZT/LSM ceramics.

It is reported that lanthanum doped PZT ceramics could get good fatigue resistance [27]. This good agreement between the lanthanum doped PZT ceramics and the LSM inserted PZT ceramics suggests that the lanthanum doping may be an important factor determining the fatigue endurance as discussed above. Moreover, for the observed improvement in fatigue endurance of the Ag||LSM/PZT/LSM||Ag capacitors, another argument [28] in support of the above analysis is provided by the lower potential energy at the interfaces for the Ag||LSM/PZT/LSM||Ag capacitor compared with the Ag||PZT||Ag capacitor, which gives rise to additional resistance to ferroelectric fatigue.

4. Conclusions

As presented in the preceding results, the introduction of a LSM buffer layer between the ceramics and the Ag electrodes can greatly improve the fatigue properties of the modified PZT ceramics. The dielectric, ferroelectric and leakage current properties observed in the Ag||LSM/PZT/LSM||Ag capacitor, indicate that the LSM buffer layer can reduce defect concentrations and limit charge injection from electrodes. A modified model for polarization fatigue has been used to explain the measured fatigue data and a good consistency between the model and the measured results is shown. Based on these results, we can deduce that the LSM buffer layer may play an important role in alleviating the accumulation of the oxygen vacancies or other point defects at the interfaces. The improved fatigue behavior could be attributed to the better interfacial characteristics between the modified PZT ceramics and the Ag electrodes.

Acknowledgments

This work was supported by the Ministry of Sciences and Technology of China through 973-Project under Grant no. 2009CB623306, the National Natural Science Foundation of China (Grant nos. 50672042 and 51072016) and the State Key, Laboratory of New Ceramics and Fine Processing (no. KF1014).

References

[1] J.F. Scott, C.A. Paz de Araujo, Ferroelectric memories, Science 246 (1989) 1400.
[2] O. Auciello, J.F. Scott, R. Ramesh, The physics of ferroelectric memories, Physics Today 51 (1998) 22.
[3] G.H. Haertling, Ferroelectric ceramics: history and technology, Journal of the American Ceramic Society 82 (1999) 797.
[4] S.R. Winzer, N. Shankar, A.P. Ritter, Designing cofired multilayer electrostrictive actuators for reliability, Journal of the American Ceramic Society 72 (1989) 2246.
[5] D.C. Lupascu, Fatigue of Ferroelectric Ceramics and Related Issues, Springer, Heidelberg, 2004.
[6] M. Grossmann, O. Lohse, D. Bolten, T. Schneller, R. Waser, The interface screening model as origin of imprint in $PbZr_xTi_{1-x}O_3$.I. dopant, illumination, and bias dependence, Journal of Applied Physics 92 (2002) 2680.
[7] R. Meyer, R. Liedtke, R. Waser, Oxygen vacancy migration and time-dependent leakage current behavior of $Ba_{0.3}Sr_{0.7}TiO_3$ thin films, Applied Physics Letters 86 (2005) 112904.
[8] E.L. Colla, I. Stolichnov, P.E. Bradely, N. Setter, Direct observation of inversely polarized frozen nanodomains in fatigued ferroelectric memory capacitors, Applied Physics Letters 82 (2003) 1604.
[9] E.L. Colla, D.V. Taylor, A.K. Tagantsev, N. Setter, Discrimination between bulk and interface scenarios for the suppression of the switchable polarization (fatigue) in $Pb(Zr,Ti)O_3$ thin films capacitors with Pt electrodes, Applied Physics Letters 72 (1998) 2478.
[10] G.S. Wang, X.J. Meng, J.L. Sun, Z.Q. Lai, J. Yu, S.L. Guo, J.G. Cheng, J. Tang, J.H. Chu, $PbZr_{0.5}Ti_{0.5}O_3/(La_{0.5}Sr_{0.5})CoO_3$ heterostructures prepared by chemical solution routes on silicon with no fatigue polarization, Applied Physics Letters 79 (2001) 3476.
[11] M. Chen, T. Wu, J. Wu, Effect of textured $LaNiO_3$ electrode on the fatigue improvement of $Pb(Zr_{0.53}Ti_{0.47})O_3$ thin films, Applied Physics Letters 68 (1996) 1430.
[12] I. Stolichnov, A. Tagantsev, N. Setter, J.S. Cross, M. Tsukada, Top-interface-controlled switching and fatigue endurance of (Pb,La)(Zr,-Ti)O_3 ferroelectric capacitors, Applied Physics Letters 74 (1999) 3552.
[13] W. Wu, K.H. Wong, C.L. Choy, Y.H. Zhang, Top-interface-controlled fatigue of epitaxial $Pb(Zr_{0.52}Ti_{0.48})O_3$ ferroelectric thin films on $La_{0.7}Sr_{0.3}MnO_3$ electrodes, Applied Physics Letters 77 (2000) 3441.
[14] G. Asano, H. Morioka, H. Funakubo, Fatigue-free RuO_2/$Pb(Zr,Ti)O_3$/RuO_2 capacitor prepared by metal organic chemical vapor deposition at 395 °C, Applied Physics Letters 83 (2003) 5506.
[15] F. Yan, Y.N. Wang, L.W. Chan, C.L. Choy, Ferroelectric properties of $(Ba_{0.5}Sr_{0.5})TiO_3/Pb(Zr_{0.52}Ti_{0.48})O_3/(Ba_{0.5}Sr_{0.5})TiO_3$ thin films with platinum electrodes, Applied Physics Letters 82 (2003) 4325.
[16] E.S. Lee, H.W. Chung, S.H. Lim, S.Y. Lee, Effect of double-sided $(Pb_{0.72}La_{0.28})Ti_{0.93}O_3$ buffer layers on the ferroelectric properties of $Pb(Zr_{0.52}Ti_{0.48})O_3$ thin films, Applied Physics Letters 87 (2005) 032903.
[17] T.K. Tseng, J.M. Wu, Chemical solution deposited $BaPbO_3$ buffer layers for lead zirconate titanate ferroelectric films, Thin Solid Films 491 (2005) 143.
[18] E.M. Alkoy, K. Uchiyama, T. Shiosaki, Improving fatigue resistance of $Pb(Zr,Ti)O_3$ thin films by using $PbZrO_3$ buffer layers, Applied Physics Letters 99 (2006) 106106.
[19] C.H. Sim, Z.H. Zhou, X.S. Gao, H.P. Soon, J. Wang, Ferroelectric and fatigue behavior of $Pb(Zr_{0.52}Ti_{0.48})O_3/(Bi_{3.15}Nd_{0.85})Ti_3O_{12}$ bilayered thin films, Journal of Applied Physics 103 (2008) 034102.
[20] J.J. Li, P. Li, G.J. Zhang, J. Yu, Y.Y. Wu, X.Y. Wen, The thickness effect of $Bi_{3.25}La_{0.75}Ti_3O_{12}$ buffer layer in $PbZr_{0.58}Ti_{0.42}O_3$/$Bi_{3.25}La_{0.75}Ti_3O_{12}$(PZT/BLT) multilayered ferroelectric thin films, Thin Solid Films 519 (2011) 6021.
[21] S. Zafar, R.E. Jones, P. Chu, B. White, B. Jiang, D. Taylor, P. Zurcher, S. Gillepsie, Investigation of bulk and interfacial properties of $Ba_{0.5}Sr_{0.5}TiO_3$ thin film capacitors, Applied Physics Letters 72 (1998) 2820.
[22] J. Miao, B.P. Zhang, K.H. Chew, Y. Wang, Improvement of ferroelectric fatigue endurance in multiferroic $(Ba_{0.5}Sr_{0.5})TiO_3$/$(Bi_{1.05}La_{0.05})FeO_3/(Ba_{0.5}Sr_{0.5})TiO_3$ sandwich structures, Applied Physics Letters 92 (2008) 062902.
[23] S.Y. Wang, X. Qiu, J. Gao, Y. Feng, W.N. Su, J.X. Zheng, D.S. Yu, D.J. Li, Electrical reliability and leakage mechanisms in highly resistive multiferroic $La_{0.1}Bi_{0.9}FeO_3$ ceramics, Applied Physics Letters 98 (2011) 152902.
[24] M. Dawber, J.F. Scott, A model for fatigue in ferroelectric perovskite thin films, Applied Physics Letters 76 (2000) 1060.

[25] J.M. Liu, Y. Wang, C. Zhu, G.L. Yuan, S.T. Zhang, Temperature-dependent fatigue behaviors of ferroelectric $Pb(Zr_{0.52}Ti_{0.48})O_3$ and $Pb_{0.75}La_{0.25}TiO_3$ thin films, Applied Physics Letters 87 (2005) 042904.
[26] S.R. Shannigrahi, H.M. Jang, Fatigue-free lead zirconate titanate-based capacitors for nonvolatile memories, Applied Physics Letters 79 (2001) 1051.
[27] Q. Jiang, W. Cao, L.E. Cross, Electric fatigue in lead zirconate titanate ceramics, Journal of the American Ceramic Society 77 (1994) 211.
[28] A.Q. Jiang, J.F. Scott, M. Dawber, C. Wang, Fatigue in artificially layered Pb(Zr,Ti)O3 ferroelectric films, Journal of Applied Physics 92 (2002) 6756.